Check for updates

Applied Research

Applied Research

RESEARCH ARTICLE OPEN ACCESS

Fabrication, Characterization, and Antimicrobial Activity of PLA/Chitosan Composites Reinforced With Sugarcane Bagasse–Derived Fillers

Akbarningrum Fatmawati[1] | Athalia Beatrice Molianto[1] | Theofilus Pranata[1] | Emma Savitri[1] | The Jaya Suteja[2]

[1]Chemical Engineering Department, Universitas Surabaya (UBAYA), Surabaya, Indonesia | [2]Mechanical Engineering Department, Universitas Surabaya (UBAYA), Surabaya, Indonesia

Correspondence: Akbarningrum Fatmawati (akbarningrum@staff.ubaya.ac.id)

Received: 21 January 2026 | **Revised:** 1 August 2026 | **Accepted:** 7 August 2026

Funding: Badan Riset dan Inovasi Nasional (BRIN), Grant/Award Number: 46/IV/KS/02/2025; Lembaga Pengelola Dana Pendidikan (LPDP), Grant/Award Number: 46/IV/KS/02/2025

Keywords: antimicrobial biopolymers | bagasse | biodegradable composites | cellulose | chitosan | polylactic acids

ABSTRACT

This study developed polylactic acid (PLA) composites reinforced with chitosan (CS) and sugarcane bagasse-derived fillers, including untreated sugarcane bagasse (SCB), ultrasound-assisted-alkaline-treated sugarcane bagasse (UASCB), and ultrasound-assisted-alkaline-acid-treated (UAASCB). The objective was to improve the structural and functional properties of PLA composites through fiber treatment and chitosan incorporation. Fiber treatments significantly increased the cellulose content and crystallinity of SCB, with the best result reaching 71.7% cellulose and 91.36% crystallinity after 30 min of 4 wt% NaOH treatment followed by 45 min of 2 N sulfuric acid treatment. Composite characterization was carried out using FTIR, XRD, SEM, and tensile testing. In this study, pure PLA showed a tensile strength of 6.69 ± 2.8 MPa and a tensile modulus of 313.26 ± 34 MPa. The PLA–CS–UASCB composite showed a comparable tensile strength (6.31 ± 4.4) MPa with a slight increase in tensile modulus (360 ± 84) MPa. In contrast, the PLA–CS–UAASCB composite displayed lower tensile strength (2.92 ± 0.2) MPa and tensile modulus (271.51 ± 27) MPa. The PLA–CS–UASCB composite demonstrated the highest antimicrobial activity, reducing the growth of *E. coli* by 20.28% and *S. aureus* by 28.33%. This research offers a promising foundation for further development of sustainable PLA-based biocomposites tailored for multifunctional and environmentally friendly applications.

1 | Introduction

The growing demand for sustainable material in industrial and medical applications has created a strong urgency to develop and adopt biocomposites as eco-friendly, renewable and biodegradable alternatives. Among various polymer options, polylactic acid (PLA) has emerged as a leading matrix in biocomposites. Polylactic acid (PLA), a biodegradable polymer produced from agricultural crop or waste, is widely used in automotive and packaging industry as well as biomedical field, including in composite form. Its biocompatibility with the human body makes this material a biomaterial option worth further investigation [1, 2]. Poly-L-lactic acid (PLLA) and poly-D-lactic acid (PDLA) are the first-generation biodegradable polymeric implant materials that do not exhibit toxic and mutagenic effects. In addition, they possess several desirable characteristics for use in tissue engineering, orthopedic applications, surgical sutures and drug-delivery systems including excellent mechanical strength, cytocompatibility, a suitable degradation rate, and good thermal stability. Furthermore, the thermoplastic nature of PLA enables its widespread use as a

This is an open access article under the terms of the Creative Commons Attribution License, which permits use, distribution and reproduction in any medium, provided the original work is properly cited.

© 2026 The Author(s). *Applied Research* published by Wiley-VCH GmbH.

polymer for 3D printing [2–4]. The tensile strength and flexural strength of L-PLA have been reported to range from 11.4 to 82.7 MPa and from 45 to 145 MPa, respectively, making PLA an excellent biomaterial for orthopedic implants [5, 6].

Despite being a promising material for bone implant applications due to its biodegradability, biocompatibility, and ease of processing, the use of PLA is limited by its poor thermal stability, low gas barrier properties, and brittleness. PLA exhibits intrinsic brittleness and low toughness (less than 10% elongation at break) [2]. These limitations can be mitigated by reinforcement with natural fibers [1, 7]. The primary component of natural fibers are cellulose, hemicellulose, and lignin. Among these, cellulose is primarily responsible for the reinforcing effect in polymer matrices due to its high surface area, high tensile strength, and good biocompatibility [4]. Consequently, natural fibers have strong potential as alternatives to synthetic fibers such as carbon and glass fibers for polymer reinforcement [4, 8]. Additional advantages of natural fibers over synthetic fibers include low density, low cost, comparable mechanical properties, reduced health risk, renewability, recyclability, and biodegradability [8]. Various natural fibers have been reported as excellent reinforcement for PLA matrices, including banana, sisal, jute, wheat, flax, straw, sugarcane, cotton, silk, bamboo, kenaf and coconut [4]. Sugarcane bagasse (SCB), a readily available byproduct of the sugar industry with cellulose content of 40%–50%, is a particularly attractive, low-cost reinforcement material with high tensile strength [9, 10].

Extensive investigations have been conducted on natural-fiber-reinforced plastics, reflecting their widespread use and significant potential across diverse engineering, industrial, and medical applications. The investigations encompass both untreated and chemically treated natural fibers. Chemical treatments are primarily intended to improve fiber-matrix interfacial adhesion and, consequently, to enhance tensile strength and elastic modulus [8, 11]. Alkali treated SCB at 30 wt% has been reported to enhance tensile and flexural strength of polyethylene by 41% and 72%, respectively, when maleic anhydride is used as a coupling agent [12]. Untreated rice husk fiber has been studied as a reinforcement for PLA, despite still yielding tensile strength lower than 67 MPA, which is the tensile strength value of neat PLA [13]. The addition of cellulose nanocrystal (CNC) at 1 wt% has improved the tensile strength of neat PLA by 18% although increasing CNC content to 2 wt% reduces the tensile strength again [14]. Microcrystalline cellulose (MCC) isolated from wheat straw is used as reinforcement for PLA and shows improved mechanical properties of neat PLA [15].

PLA is widely employed in tissue engineering and orthopedic implants. Consequently, PLA-based biocomposites with enhanced antibacterial properties is of critical importance. Chitosan (CS) is a linear polysaccharide which is derived from chitin, a natural polysaccharide found in the exoskeleton of insects, fungal cell wall, arthropods, and marine crustaceans. Its structure consists of two repeating subunits: N-acetylated-D-glucosamine and $\beta(1 \rightarrow 4)$ linked D-glucosamine [16, 17]. The amino group (NH_3^+) of CS can form electrostatic interactions with bacterial cell surface, thereby conferring antibacterial properties to CS [18]. Being known for its antimicrobial activity against both Gram-positive and Gram-negative bacteria, CS can therefore be incorporated into PLA-based composites to further enhance their biological functionality [19].

To date, PLA–Chitosan–treated-SCB fiber biocomposites have not been systemically investigated despite their promising potential. In this work, the properties of PLA–chitosan–treated SCB composites are examined. The effects of ultrasonic wave-assisted alkali treatment, as well as subsequent acid treatment, on SCB and their relationship to the mechanical properties of PLA–Chitosan–treated-SCB fiber are evaluated. In addition, the antibacterial performance of the reinforced composites against Gram-positive and Gram-negative bacteria is assessed.

2 | Materials and Methods

2.1 | Materials

Sugarcane bagasse (SCB) was obtained from sugar factory in Malang, Indonesia. Chitosan (degree of deacetylation > 75%, low molecular weight 50–190 kDa) was supplied by Sigma Aldrich. Polylactic acid (PLA) pellet (PT. Citra Murti Selaras and Edic Gripseddas, Tangerang, Indonesia) were used as the polymer matrix. Sodium hydroxide (NaOH) pellets (Merck Millipore) and sulfuric acid (H_2SO_4, 95%, Mallinckrodt) were used for pretreatment. Nutrient Broth (NB), Nutrient Agar (NA), Plate Count Agar (PCA) media, and buffered peptone water (BPW) used for microbial analysis were purchased from Merck (GranuCult, Darmstadt, Germany). *Staphylococcus aureus* (Gram-positive) and *Pseudomonas aeruginosa* (Gram-negative) were used as test organisms [19].

2.2 | Preparation of SCB Particles

Sugarcane bagasse was washed thoroughly to remove impurities. The washed bagasse was then subsequently sun-dried. The dried SCB was subsequently ground into powder using a disk mill machine (FFC type 23 A, with a speed of 5800 rpm, power 3 kW, Shandong Ji Mu Disk Mill Machinery), as described by Fatmawati et al. [20]

2.3 | Particle Size Analysis of SCB

The milled SCB was weighed and subjected to particle size distribution analysis using a standard sieve set (Retsch, Germany). Sieving was performed sequentially from the largest to the smallest mesh sizes, with a collection pan positioned at the bottom. The process was continued until no further change in mass was observed for any sieve or the pan, ensuring complete separation of particle fraction. The retained mass on each sieve was recorded, and the particle size distribution was calculated as the mass fraction of each size range relative to the total sample mass. The dry SCB powder used in this study consisted of particles in the size range of 0.4–1.41 mm (73%), 0.21–0.4 mm (13.45%), and < 0.074 mm (4.45%).

2.4 | Experiment Design of SCB Pretreatment

The overall experimental procedure in this study is illustrated in Figure 1. Alkaline pretreatment was conducted using various

27024288, 2026, 4, Downloaded from https://onlinelibrary.wiley.com/doi/10.1002/appl.70161 by Akbarningsum Fatmawati - Nat Prov Indonesia , Wiley Online Library on [18/08/2026]. See the Terms and Conditions (https://onlinelibrary.wiley.com/terms-and-conditions) on Wiley Online Library for rules of use; OA articles are governed by the applicable Creative Commons License

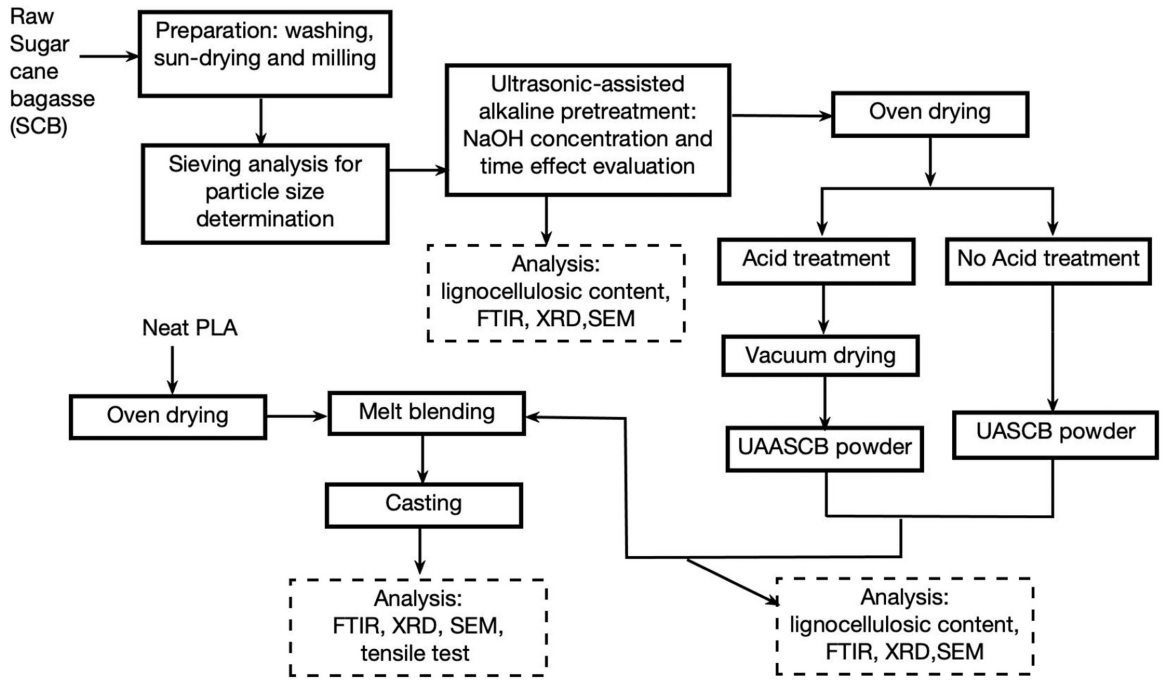

FIGURE 1 | Schematic diagram of experimental methodology used in this study.

TABLE 1 | Formulation and variation in composite composition.

Composite sample	PLA, wt%	CS, wt%	Untreated- or treated-SCB, wt%
Neat PLA	100	0	0
PLA–CS	99	1	0
PLA–CS–SCB	96	1	3
PLA–CS–UASCB	96	1	3
PLA–CS–UAASCB	96	1	3

NaOH concentrations of 0% (water–treated), 4%, 8%, and 12% (wt/wt) for 30 min. Based on the result of this step, the optimum NaOH concentration, determined from the maximum cellulose content of the treated SCB powder, was selected to investigate the effect of different Ultrasonic-assisted (UA) treatment times of 15, 30, 45, and 60 min. Subsequently, the treatment condition, defined by NaOH concentration and treatment time that yielded the highest cellulose content in the treated SCB powder, was chosen for further processing prior to acid treatment. Acid treatment was then carried out using 2 N H_2SO_4 for 30 min. All experiments were carried out in duplicates.

2.5 | Alkaline Pretreatment With Ultrasonic Assistance

Milled SCB powder was mixed with 300 mL of 4% (wt/wt) NaOH solution at a solid-to-liquid ratio of 1:20 (g/mL). The suspension was sonicated for 30 min using a 20 kHz ultrasonic bath. Following treatment, the slurry was filtered through filter paper, and the solid residue was thoroughly washed with distilled water until a neutral pH was attained. The washed residue was subsequently dried at 50^oC until a constant mass was achieved. The same procedure was repeated using NaOH concentrations of 0%, 8%, and 12%, as well as for sonication times of 15, 45, and 60 min.

2.6 | Acid Hydrolysis

A 2 N Sulfuric acid solution (100 mL) was prepared, and 10 g of cellulose obtained from the alkaline pretreatment was weighed. The cellulose was then mixed with 100 mL of 2 N H_2SO_4 and subjected to hydrolysis under reflux at 45^oC for 45 min. Following hydrolysis, the suspension was filtered, and the solid residue was washed with distilled water until neutral pH was achieved. The washed material was subsequently dried in a vacuum oven at 50^oC until constant mass was obtained.

2.7 | Composite Fabrication

The composite formulation was prepared according to Table 1. All materials were dried at 80^oC for 4 h prior to blending. After drying the materials with a total mass of 25 g were blended, placed within stainless steel cup and heated in a glycerol bath to

27024288, 2026, 4, Downloaded from https://onlinelibrary.wiley.com/doi/10.1002/appl.70161 by Akbarningrum Fatmawati - Nat Prov Indonesia , Wiley Online Library on [18/08/2026]. See the Terms and Conditions (https://onlinelibrary.wiley.com/terms-and-conditions) on Wiley Online Library for rules of use; OA articles are governed by the applicable Creative Commons License

maintain a mixing temperature of 180^oC for 25 min. The mixture was stirred using a stainless-steel impeller at 50 rpm. The blended mixture was then transferred into an ASTM D638 type I test specimen silicone mold, with the mold specifications as described by Suteja et al. [21]

2.8 | Analysis Methods

2.8.1 | *Chemical Composition Analysis*

The chemical composition of untreated and treated SCB fibers was determined using the Chesson-Datta gravimetric method [22, 23]. This procedure quantified water-extractive, cellulose, hemicellulose, and lignin contents through sequential extraction, filtration, drying, and spent–solid weight measurement of the raw and treated SCB powders. Each analysis was performed in duplicates.

2.8.2 | *Composites Characterization*

Chemical structures were analyzed using Fourier-Transform Infrared (FT-IR) spectroscopy (FTIR) to identify functional group. The FTIR was performed on SHIMADZU IRTracer–100 instrument, and FTIR spectra were recorded in the range of 4000–400 cm^{-1}.

The material crystallinity was determined from diffractograms obtained from Xray diffraction (XRD) using Cu Kα radiation over a 2θ range from $10^o - 50^o$. The morphology of untreated SCB, treated SCB, and the resulting composites was examined via scanning electron microscopy (SEM). The crystallinity of untreated SCB and treated SCB was evaluated using Segal method, which employs the ratio of the crystalline peak ($I_{002} - I_{am}$) to the total intensity (I_{002}), as expressed in **Equation** 1 [24, 25]. Peak intensities were evaluated after peak smoothing using Savitzky-Golay filter and background subtraction was fitted using cubic spline.

$$\% CI = \left(\frac{I_{002} - I_{am}}{I_{002}}\right) \times 100. \quad (1)$$

The crystallinity the composites was evaluated using **Equation** 2, where A_{am} is the area of the amorphous hump and A_{total} is the total area of all peaks [26].

$$CI\ (\%) = \left(1 - \frac{A_{am}}{A_{total}}\right) \times 100. \quad (2)$$

The amorphous region was fitted using a cubic spline. The areas of crystalline peak and amorphous hump were calculated by trapezoidal integration. All smoothing, background subtraction, fitting, and area calculations were performed using MATLAB R2021b.

The mechanical properties of PLA–CS–SCB composites were evaluated by tensile testing to determine tensile strength and elastic modulus using universal testing machine according to ASTM E638-22, standard test method for tensile properties of plastics [14, 21].

2.8.3 | *Antimicrobial Activity*

Antimicrobial performance against *Escherichia coli* and *Staphylococcus aureus* was evaluated under dynamic contact condition, based on ASTM E2149 [27, 28]. Both bacterial strains were maintained on NA plates. Prior to the antimicrobial activity assay, each culture was grown in NB medium by transferring a single loopful colony from NA plate and incubating for 18 h at 35°C to obtain approximately 10^7 CFU/mL. The resulting broth cultures were then diluted in BPW. Subsequently, 1 g of composites was added to 50 mL of inoculated nutrient broth and incubated for 1.5 h under agitation at 100 rpm. One milliliter of the incubated broth was serially diluted in BPW and mixed with melted PCA using the pour plate technique. The plates were incubated at 35°C for 24 h before colony enumeration. The percentage reduction in bacterial growth was determined from colony counts (CFU/mL) relative to the control group, defined as inoculated nutrient broth without composite, using the following equation [29]:

$$\% R = \frac{N_0 - N}{N_0} \times 100, \quad (3)$$

where N_0 is the initial bacterial count in the broth and N is the count after incubation with composite sample.

2.9 | Statistical Analysis

All experiments in this study were conducted in duplicate, and the reported measurements and calculations were based on the corresponding mean values. Statistical analysis of the SCB treatment was performed using (ANOVA) Microsoft Excel.

3 | Results and Discussion

The particle size distribution analysis revealed that sugarcane bagasse particle was predominantly composed of particles in the 14/40 mesh size range, accounting for 73.3% of the total mass. The 40/70 mesh fraction represented 13.45%, while all finer particle sizes contributed less than 5% each. The marked predominance of coarse particles indicates that larger particle sizes dominate the raw material.

3.1 | Effect of Ultrasound-Assisted Alkaline Pretreatment on Cellulose Content

Figure 2 shows that raw SCB consists of 43.2 wt% cellulose, 31.7 wt% hemicellulose, 10.7 wt% lignin, 10.3 wt% water-extractives, and the remainder ash. The high cellulose content highlights its potential as a lignocellulosic feedstock for producing commercial cellulose derivatives such as CNC and MCC. The figure also shows that bath ultrasound-assisted alkaline (UA) treatment using NaOH (0–12%) effectively increased cellulose content while reducing hemicellulose and lignin levels. The ANOVA results ($p < 0.05$) confirmed that NaOH concentration significantly influenced the chemical composition. Increasing the NaOH concentration up to 12% led to an increase in cellulose content to 54.6 ± 0.7%. However, the maximum cellulose content of 58.9 ± 3.7% was achieved with UA

27024288, 2026, 4, Downloaded from https://onlinelibrary.wiley.com/doi/10.1002/appl.70161 by Akbarningrum Fatmawati - Nat Prov Indonesia , Wiley Online Library on [18/08/2026]. See the Terms and Conditions (https://onlinelibrary.wiley.com/terms-and-conditions) on Wiley Online Library for rules of use; OA articles are governed by the applicable Creative Commons License

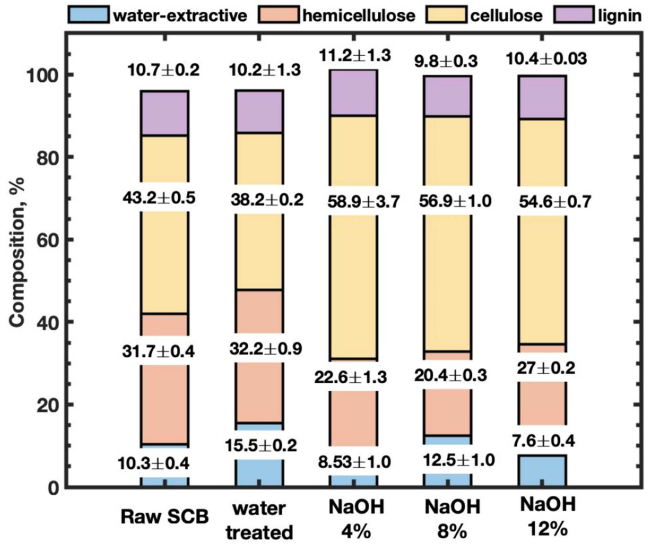

FIGURE 2 | Effect of ultrasound-assisted alkaline treatment at varied NaOH concentration on the SCB cellulose content.

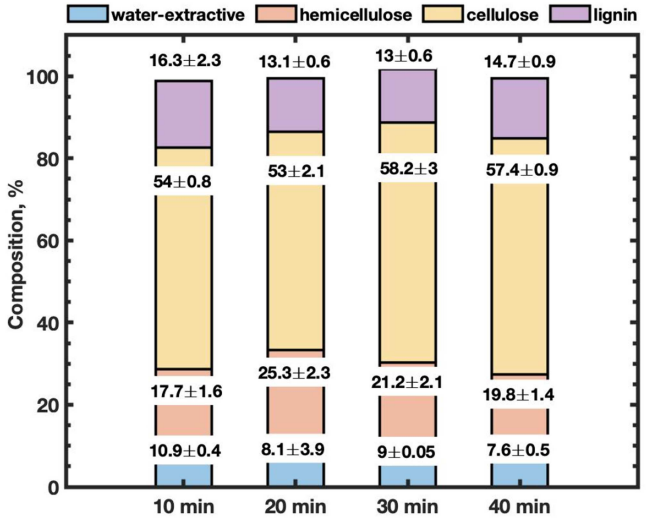

FIGURE 3 | Effect of UA alkaline treatment time on the SCB cellulose content.

treatment at NaOH concentration of 4%. Similarly, Gavrilla et al., employed bath ultrasound-assisted alkaline pretreatment and achieved 57% higher delignification compared to conventional alkaline pretreatment [30].

The increase in cellulose content arises from the action of ultrasonic waves, which create alternating compression and rarefaction cycles in the liquid medium and thereby induce cavitation bubble formation. Upon collapse, these bubbles generate localized hot spots (~5000 K, ~2000 atm) that disrupt lignocellulosic matrix, degrade crystalline cellulose, lyse cell walls, and promote organic matter solubilization [31]. Because of its amorphous nature, hemicellulose, is more susceptible to degradation than crystalline cellulose, which leads to a relative enrichment of cellulose in the biomass following treatment. Alkaline treatment also cleaves the ester bonds in lignin-cellulose complexes, solubilizing lignin and thereby increasing cellulose content while reducing hemicellulose and lignin levels [32]. However, at higher alkali concentration, cellulose chain begin to break, limiting the net cellulose content, consequently the maximum cellulose content is achieved at a NaOH concentration of 4%. Peng, et al. reported that higher NaOH concentrations lead to the formation of smaller hydrate molecules, which can readily enter the cellulose structure and form hydrogen bond with cellulose. This process disrupts the original hydrogen-bond network of cellulose and ultimately leads to cellulose dissolution [33].

Figure 3 shows the composition of SCB after treatment with a 4% NaOH solution at various sonication times. The data demonstrate that the removal of hemicellulose and lignin increased the cellulose content. The highest cellulose content was obtained at 30 min, which represents the optimal delignification condition. Extending the treatment to 40 min caused a reduction in cellulose content, most likely due to cellulose dissolution and the loss of soluble components. A similar phenomenon is also observed in the alkaline cellulose extraction from empty palm oil fruit bunch and jack fruit leaves, as reported by Tristantini et al. [34] Longer contact time with alkaline cause the decrease in hemicellulose and lignin content, which lead to the increase in alkali accessibility to cellulose structure. This can disrupt the hydrogen-bond of cellulose and lead to dissolution as explained above. Previous work on alkaline treatment of sugar palm fiber reported a decrease in cellulose content at prolonged treatment [35]. The ANOVA ($p > 0.05$) result indicates that the selected time range does not have a significant effect on cellulose content.

3.2 | Effect of Acid Treatment on the Cellulose Content of UA-Alkaline-Treated-SCB

Acid treatment is used to produce microcrystalline cellulose (MCC) from SCB–derived cellulose obtained by delignification. After alkaline delignification, the amorphous part of cellulose can be selectively degraded by acid hydrolysis, resulting in a more crystalline material with high rigidity that is suitable for use as a reinforcing agent [36]. The treatment is carried out because MCC has a large specific surface area, which enhances the interaction between the matrix and the reinforcing material, thereby improving the mechanical properties [15]. Figure 4 shows the effect of subsequent sulfuric acid treatment on the composition of SCB. Acid hydrolysis with H_2SO_4 selectively degrades hemicellulose by cleaving glycosidic bonds in the amorphous regions and can also solubilize portions of lignin through bond breakage, while the crystalline cellulose fraction remains comparatively stable. Consequently, the cellulose content can increase significantly. Following acid treatment, the cellulose content of UA-treated SCB increases markedly. Adel et al. also reported that combined sonication and acid pretreatment produced the highest degree of delignification and the greatest enrichment of cellulose content in rice hulls and bean hulls compared with untreated material or sonication alone [37].

3.3 | FT-IR Analysis

FT-IR spectra of raw SCB, ultrasound-assisted-alkaline-treated SCB (UASCB) and ultrasound–assisted–alkaline–acid-treated

27024288, 2026, 4, Downloaded from https://onlinelibrary.wiley.com/doi/10.1002/appl.70161 by Akbarningrum Fatmawati - Nat Prov Indonesia , Wiley Online Library on [18/08/2026]. See the Terms and Conditions (https://onlinelibrary.wiley.com/terms-and-conditions) on Wiley Online Library for rules of use; OA articles are governed by the applicable Creative Commons License

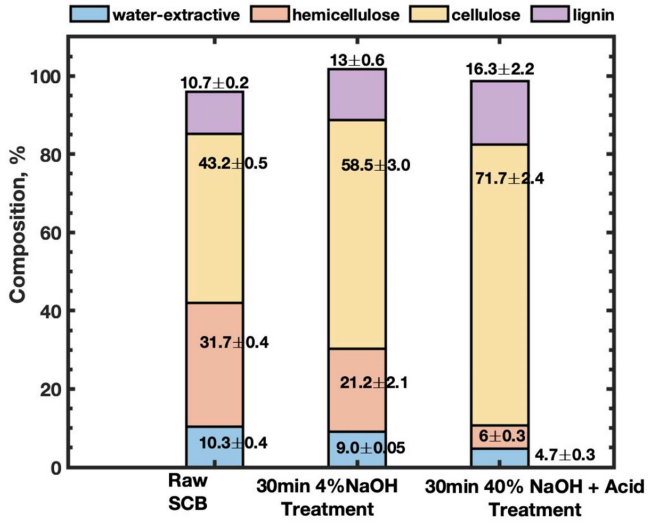

FIGURE 4 | Effect of acid treatment on the UA-alkaline-treated SCB composition.

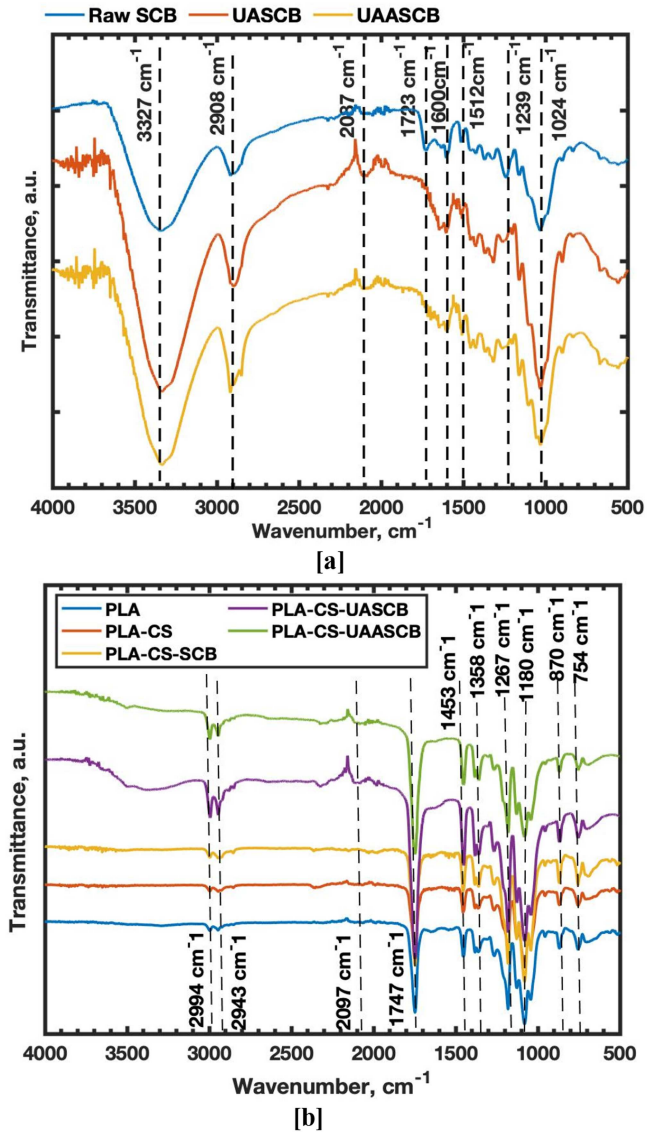

FIGURE 5 | FTIR spectra of (a) treated SCB and (b) PLA composites.

SCB (UAASCB) are shown in Figure 5a. The three samples display two main absorption regions at high wavenumber ($3500 - 2800 cm^{-1}$) and low wavenumbers ($1700 - 500 cm^{-1}$), respectively. They have similar FTIR spectra peak curve, which demonstrated that their chemical compositions are similar throughout the chemical treatment. The broad absorption band at 3336 and 1603 cm^{-1} shows —OH stretching and bending vibration. The peak at 3336 cm^{-1} represents the presence of hydrogen bonded —OH bond in cellulose, hemicellulose and lignin [38, 39]. This peak is narrowed but shows higher intensity after treatment. This indicates that stronger —OH vibration and may imply increase crystallinity as amorphous constituents such as hemicellulose and lignin are partly eliminated during the treatment. This is also caused by more ordered cellulose chain and less water absorbed [40, 41]. Absorption at 2910 cm^{-1} shows symmetry and asymmetry stretching vibration from CH_2. Peak at 1159 cm^{-1}shows an absorption of asymmetry C—O—C bond. Whereas the absorption at 1031 cm^{-1} and 897 cm^{-1} shows C—O—C bond stretching at beta–(1,4)–glycosidic [15]. The absorption band at 1423 cm^{-1} represented C—H bending vibration [14]. Additionally, a peak at 1723 cm^{-1} [37], assigned to C═O stretching of ester groups in lignin and hemicellulose, was observed in SCB samples but absent in the other two samples, confirming partial removal of these components. The band at 1024 cm^{-1} (C—O bond vibration) also shows more intense for after treatment as other non-cellulosic components are removed yielding more ordered cellulose structure and hence increase crystallinity [41].

The FTIR of PLA composites in this study is shown in Figure 5b. The broad absorption at 3369 cm^{-1} shows stretching vibration of —OH and N—H bond of chitosan and cellulose [29]. At 2995 cm^{-1} and 2945 cm^{-1} shows the symmetry and asymmetry of CH_3 stretching vibration. A strong peak at 1747 cm^{-1} indicates C═O bond from keto ester of PLA [42]. Meanwhile, at 1080 cm^{-1} and 1042 cm^{-1} indicates stretching of C—O. The absorption band at 869 cm^{-1} represented beta–(1–4)–glycosidic bending [15, 43]. The interaction between PLA, SCB, and chitosan is observed at the peak of 3369 cm^{-1}, indicating hydrogen bonding between PLA and chitosan as well as between PLA and cellulose [42, 43].

3.4 | X-Ray Diffraction of Treated SCB and Composites

The X-ray diffraction patterns of the raw SCB, UA-alkaline treated SCB (UASCB), and UA alkaline and acid treated SCB (UAASCB) are illustrated in Figure 6a. The figure indicates that sugarcane bagasse contains both crystalline and amorphous regions. A strong diffraction peak was observed at $2\theta = 22^o$, a smaller peak at $2\theta = 34^o$, and a secondary peak adjacent to the main peak at $2\theta = 15 - 19^o$, which are characteristic of crystalline cellulose. The sharper crystalline peaks after treatment indicate an increase in the degree of crystallinity, suggesting partial removal of amorphous components such as hemicellulose and lignin.

The crystallinity index (CI) of SCB increased progressively with each treatment, from 64.7% in SCB to 88.95% after ultrasound-assisted alkaline treatment and finally reached a maximum of

27024288, 2026, 4, Downloaded from https://onlinelibrary.wiley.com/doi/10.1002/appl.70161 by Akbarningrum Fatmawati - Nat Prov Indonesia , Wiley Online Library on [18/08/2026]. See the Terms and Conditions (https://onlinelibrary.wiley.com/terms-and-conditions) on Wiley Online Library for rules of use; OA articles are governed by the applicable Creative Commons License

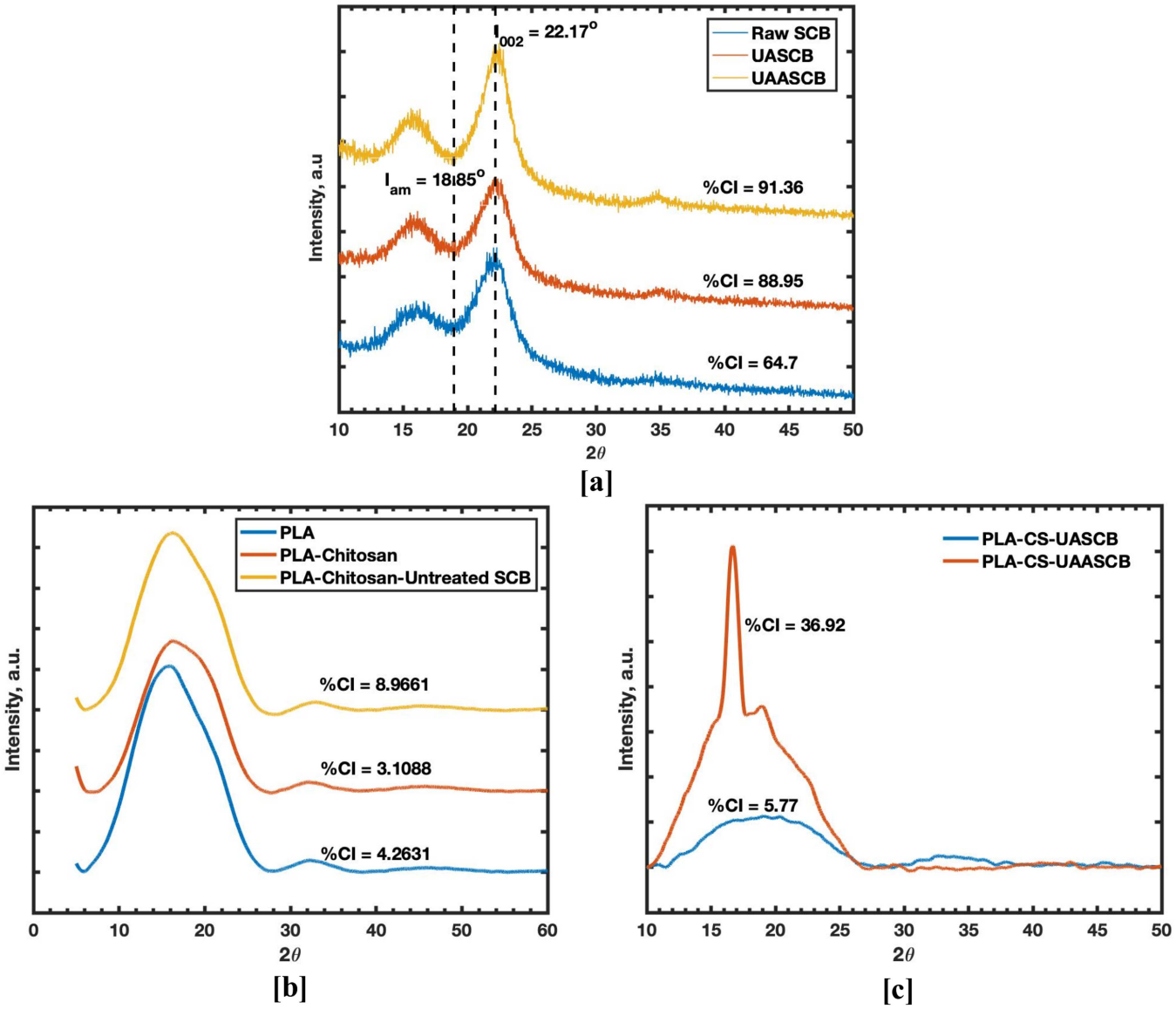

FIGURE 6 | X-ray diffraction (XRD) patterns of (a) untreated and treated SCB and (b and c) PLA-based composites.

91.36% following acid treatment. These high crystallinity values of treated SCB show the formation of high degree of structural order, as reported by Techawinyutham et al. [44] The increasing trend in CI values of treated SCB demonstrates that both UA alkaline and acid treatments are effective in reducing the amorphous fraction of cellulose [45]. This is because the UA alkaline treatment removes amorphous hemicellulose and lignin, whereas the subsequent acid treatment causes degradation of remaining amorphous SCB, as described in **Subsections 3.1. and 3.2**. The enhancement in crystallinity is likely due to reagent penetration into the the amorphous regions, resulting in cleavage of glycosidic bonds, as reported by Maslennikov, et al. [46]

Crystallinity relates to the degree of structural order in a material. Crystallinity is an important property of polymers, as crystalline polymers typically exhibit good mechanical strength, low gas permeability, low gas permeability (particularly oxygen and carbon dioxide), and thermal stability [47–49]. Figure 6b and Figure 6c shows the XRD diffractograms of the composites. Figure 6b illustrates the predominantly amorphous character of PLA, PLA−CS, and PLA−CS−SCB composites. Incorporation of UAASCB into PLA diminishes the characteristic crystalline peak of SCB at $2\theta = 22.17^{o}$ and gives rise to a very small new peak near $2\theta = 16.71°$, which corresponds to the a crystalline PLA peak reported by Mazzanti, et al. [50] This indicates the presence of interactions between PLA and other constituents of the composites [15, 37]. Rapid cooling of neat PLA specimens after melting results in low crystallinity [50]. The crystallinity of PLA–CS–UASCB composite is 5.77%, whereas that of PLA–CS–UAASCB is 36.92%. This difference may be attributed to the additional acid treatment applied to UASCB, which increases the crystallinity of UAASCB (Figure 6a) and consequently enhances the crystallinity of the corresponding composite. The addition of cellulose can increases the crystallinity of PLA because the high surface area of cellulose can induce a stronger heterogeneous nucleation effect on PLA, as reported by Yu, et al. [51] The very low crystallinity of PLA–CS–UASCB is consistent with that of PLA/banana fiber biocomposites reported by Komal et al. [52] This low crystallinity suggests that entanglement of the filler components (CS and UASCB)

27024288, 2026, 4, Downloaded from https://onlinelibrary.wiley.com/doi/10.1002/appl.70161 by Akbarningrum Fatmawati - Nat Prov Indonesia , Wiley Online Library on [18/08/2026]. See the Terms and Conditions (https://onlinelibrary.wiley.com/terms-and-conditions) on Wiley Online Library for rules of use; OA articles are governed by the applicable Creative Commons License

restricted the conformational freedom of PLA chains, which is essential for ordered crystal formation [53]. The amorphous XRD pattern of PLA–CS–UASCB composite is in agreement with that of PLA–hemp fiber composites demonstrated by Mazzanti [50].

3.5 | Morphologies of Treated SCB and Composites

The scanning electron microscopy (SEM) images of SCB, UASCB, and UAASCB are presented in Figure 7. SEM observations of SCB show clear morphological differences among the various treatments. The untreated SCB displays a relatively smooth surface, with only a few visible fragments likely generated during the milling process. The particles are generally compact with a sooth morphology and limited porosity. In contrast sonication in 4 wt% NaOH disrupts the SCB fibers and promotes extensive removal of hemicellulose and lignin, leading to the development of voids and a much rougher surface texture [54]. In addition, disruptions or fibrillation results of the fiber surfaces increase the available fiber surface area [38, 55]. As described in **Subsections 3.1.**, ultrasonic irradiation generates collapsing bubbles that release sufficient energy to cleave the fibers, remove non-cellulosic components, and thereby induce voids formation and surface roughening. Indeed, this increased roughness, together with high aspect ratio enhances interfacial adhesion in composite fabrication, as reported by Techawinyutham et al. [44] Some particles appeared fractured, and residual non-cellulosic materials partially covered their surfaces, indicating incomplete lignin removal due to protective waxy layers and hydrophobic compounds, as described by Ko et al. [54] SEM image of UASCB indicates that subsequent acid treatment further degrades lignin and hemicellulose, resulting in larger voids and cracks as well as rougher surface morphology. This effect is attributed to penetration into amorphous cellulose regions and cleavage of the $\beta - 1{,}4 -$ linkages between repeating units [44].

SEM images of the tensile fracture surface PLA and its composites (Figure 8) reveal the presence of voids, filler agglomeration, and interfacial gaps, despite indications of

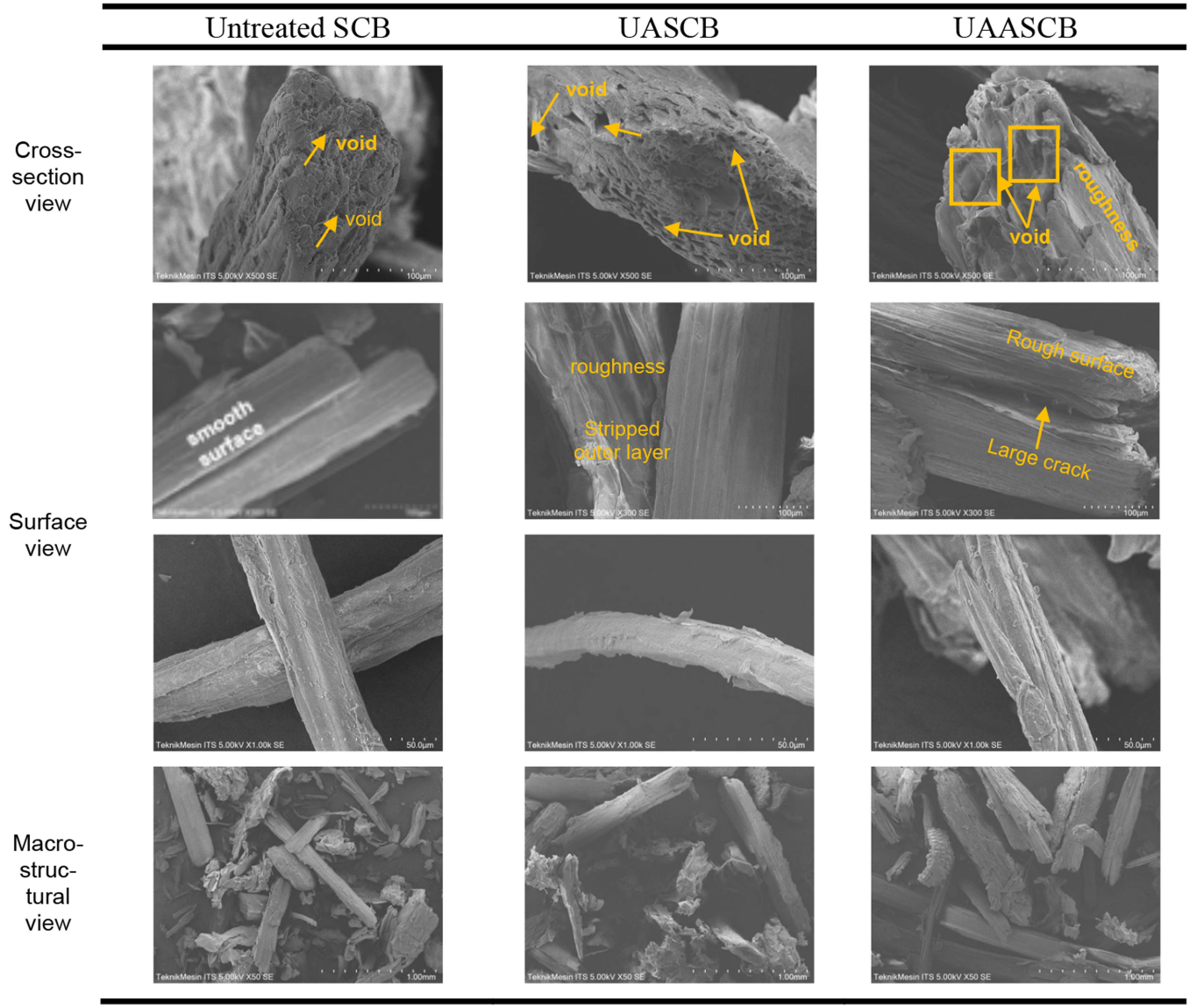

FIGURE 7 | SEM images of untreated SCB, UASCB, and UAASCB.

27024288, 2026, 4, Downloaded from https://onlinelibrary.wiley.com/doi/10.1002/appl.70161 by Akbarningrum Fatmawati - Nat Prov Indonesia , Wiley Online Library on [18/08/2026]. See the Terms and Conditions (https://onlinelibrary.wiley.com/terms-and-conditions) on Wiley Online Library for rules of use; OA articles are governed by the applicable Creative Commons License

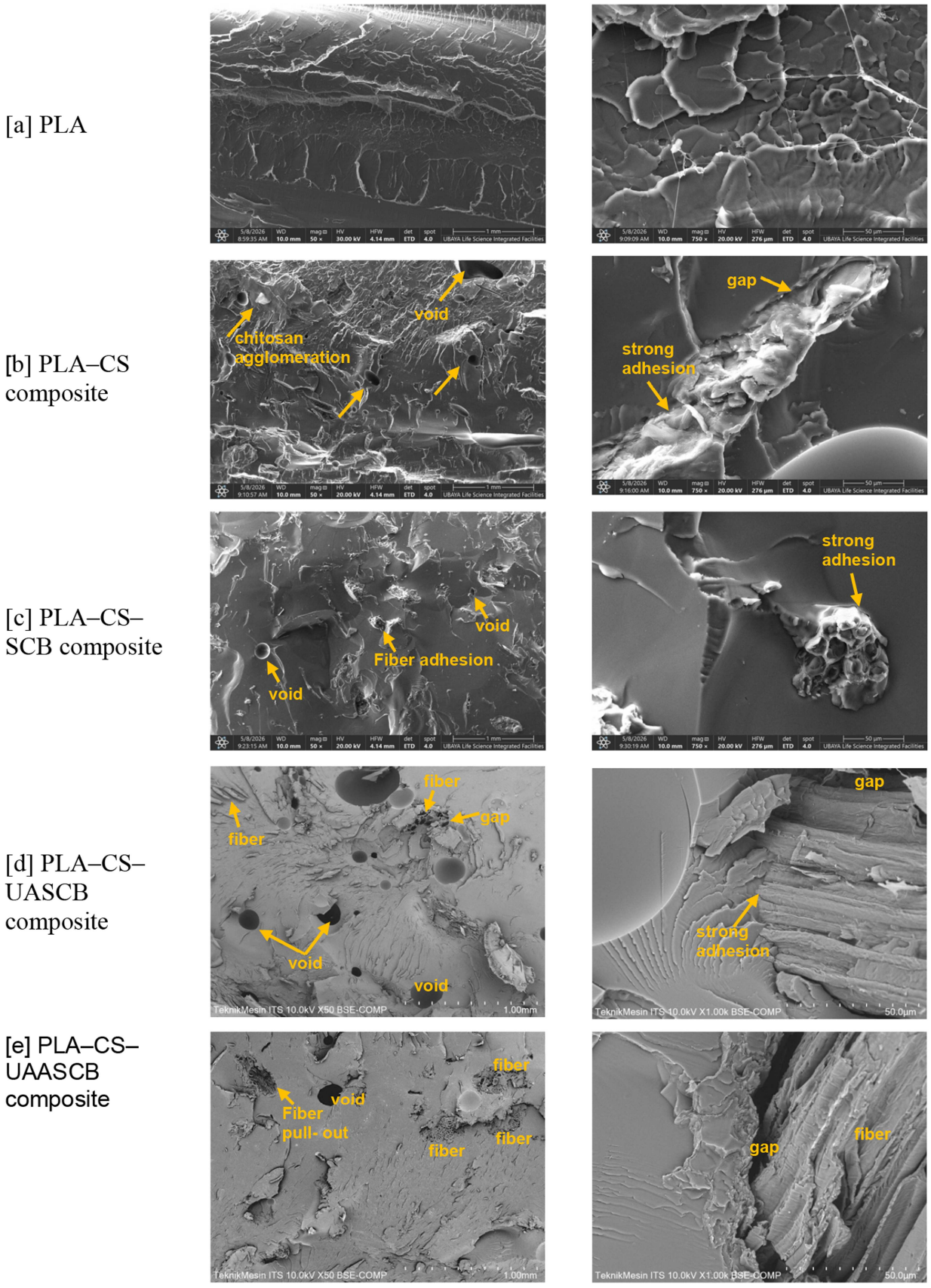

FIGURE 8 | SEM images of the tensile fracture surfaces of PLA and its composites. (a) PLA. (b) PLA–CS composite. (c) PLA–CS–SCB composite. (d) PLA–CS–UASCB composite. (e) PLA–CS–UAASCB composite.

27024288, 2026, 4, Downloaded from https://onlinelibrary.wiley.com/doi/10.1002/appl.70161 by Akbarningrum Fatmawati - Nat Prov Indonesia , Wiley Online Library on [18/08/2026]. See the Terms and Conditions (https://onlinelibrary.wiley.com/terms-and-conditions) on Wiley Online Library for rules of use; OA articles are governed by the applicable Creative Commons License

strong adhesion. The fracture surface of neat PLA appears relatively smooth compared to the composites. In the PLA–CS composite, pronounced chitosan agglomeration is observed. Both strong adhesion and gap are observed around the agglomerate. The fracture surface of PLA–CS–SCB shows relatively smoother than those of PLA–CS–UASCB and PLA–CS–UAASCB, although small voids are still present. Fiber agglomeration accompanied by strong adhesion is evident in the micrographs. In contrast, the PLA–CS–UASCB and PLA–CS–UAASCB composites exhibit more pronounced interfacial gaps and voids. These observations may be attributed to the non-compressive molding method and the relatively large fiber size. Previous studies have reported that reducing fiber dimensions and employing compression molding are necessary to mitigate the formation of voids [43, 56]. A tensile fracture surface SEM image showing excellent interfacial adhesion in alkali-treated-SCB-reinforced low-density polyethylene (LDPE) with maleic anhydride as a coupling agent was reported by Saber, et al. [12] In that study, alkali treatment improved the interfacial bonding of composites produced via injection molding. Furthermore, alkali treatment without a coupling agent has been shown to remove waxes from bagasse fiber and promote strong interactions between the fibers and LDPE [8].

3.6 | Tensile Property of the Composites

Tensile specimens fabricated from PLA and its composites exhibit different colors, which may be attributed to the characteristics of fillers and the pretreatment applied to the reinforcing fibers. Figure 9 shows the tensile specimens of PLA and its composites. PLA specimen (Figure 9a) shows a transparent appearance, whereas the composites appear opaque (Figure 9b–d). The dark brown color of PLA–CS–SCB composite may be attributed to the native lignin in SCB that has not been removed. Alkaline treatment removes a significant portion of the lignin in SCB and consequently results in the yellowish–brown color of the PLA–CS–UASCB composite. The PLA–CS–UAASCB composite appears black, which may be due to the presence of residual H_2SO_4 within the fiber pores that can act as a catalyst for carbonization during melt processing, thereby producing black char [57]. Banerjee et al. fabricated fiber–reinforced PLA composite using alkaline-treated flax and pinecone fibers via hot compression molding, yielding specimens with a translucent amber–brown matrix color and clearly visible fibrous inclusions [58]. Techawinyutham et al. prepared rice husk subjected to successive alkali–acid–bleaching treatment for epoxy reinforcement and obtained specimens with opaque medium to dark brown color [44].

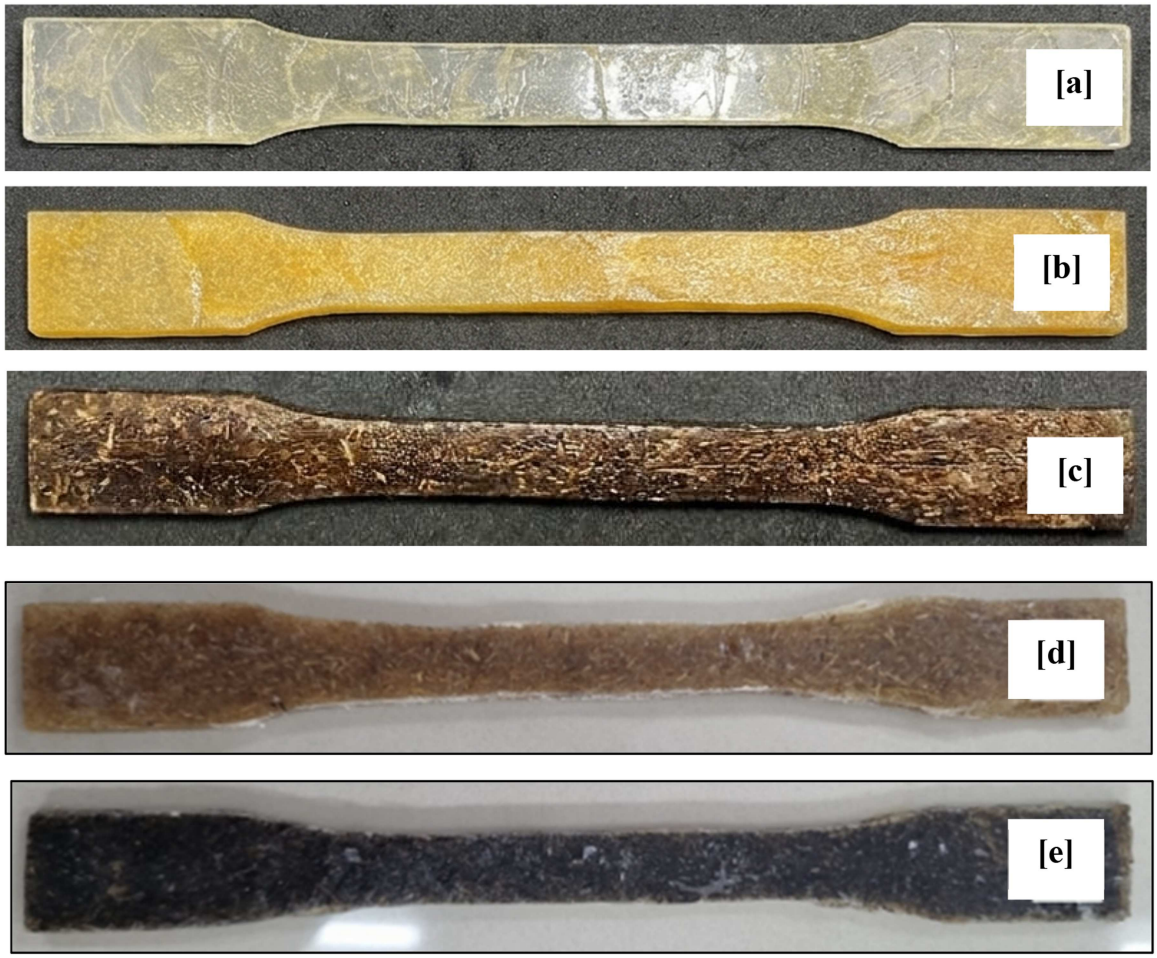

FIGURE 9 | Photographs of the prepared specimens: (a) PLA, (b) PLA–CS, (c) PLA–CS–SCB, (d) PLA–CS–UASCB, and (e) PLA–CS–UAASCB.

27024288, 2026, 4, Downloaded from https://onlinelibrary.wiley.com/doi/10.1002/appl.70161 by Akbarningrum Fatmawati - Nat Prov Indonesia , Wiley Online Library on [18/08/2026]. See the Terms and Conditions (https://onlinelibrary.wiley.com/terms-and-conditions) on Wiley Online Library for rules of use; OA articles are governed by the applicable Creative Commons License

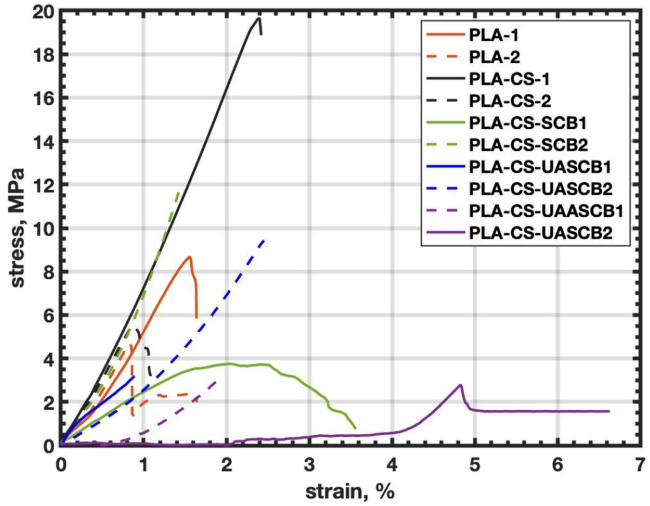

FIGURE 10 | Stress-strain curve of the experiment specimens.

TABLE 2 | The tensile strength and modulus of the experiment specimen.

Composite	Tensile strength (MPa)	Tensile modulus (MPa)
Neat PLA	6.69 ± 2.8	313.26 ± 34
PLA–CS	12.60 ± 10	546.35 ± 74
PLA–CS–SCB	7.73 ± 5.6	384.21 ± 205
PLA–CS–UASCB	6.31 ± 4.4	360.02 ± 84
PLA–CS–UAASCB	2.92 ± 0.2	271.51 ± 27

Figure 10 shows stress–strain curves of the fabricated composite specimens, which exhibit distinct stress–strain behaviors. The corresponding tensile strength and tensile modulus values are summarized in Table 2. The PLA specimens (dashed and solid red lines) show a clear yield strength point followed by strain–softening. Similar strain softening behavior in PLA has been reported by Mokhena et al. [59] However, other studies have described PLA as exhibiting ductile behavior, characterized by a necking and plateau region after short strain softening [13, 50, 60, 61]. The tensile strength and tensile modulus of the PLA specimens in this study are approximately one order of magnitude lower than the values reported in the literature, which are 50–70 MPa and 3 GPa, respectively [58]. This reduction may be attributed to PLA chain scission during open heating. The shortening of the polymer chain may result from by hydrolytic or thermo-oxidative degradation caused by exposure to air and moisture at high temperature. Consequently, these degradation mechanisms lead to decreases in tensile strength and tensile modulus [62, 63]. Nevertheless, another study on the mechanical properties of 3D–printed PLA and similarly reported a low tensile strength of 9.45 MPa and a tensile modulus of 415 MPa [64]. Strain–softening behavior is also observed in PLA–CS composite specimens (dashed and solid black lines). These composites exhibit the highest tensile strength and modulus. In contrast, two PLA–CS–SCB specimens (dashed and solid green lines) show different behavior. One specimen exhibits brittle with relatively higher tensile stress and stiffness, indicating limited capacity for energy absorption through plastic deformation (dashed green line). Meanwhile, the other specimen shows non-linear elastic behavior followed by a plateau and subsequent strain softening, indicating a less rigid material (solid green line). Owing to this contrasting deformation, the average tensile strength and elastic modulus of PLA–CS–SCB are higher than those of neat PLA. Two specimens of PLA–CS–UASCB exhibits its brittle behavior, as indicated by the presence of only elastic region (dashed and solid blue lines), although one specimen shows higher tensile strength than the other. The PLA–CS–UAASCB composite also shows two different behaviors. The first specimen is brittle and exhibits low tensile strength, whereas the second specimen shows a nonlinear elastic behavior followed by strain-softening in the plastic region. Overall, the stress-strain behavior observed in the tested specimens reflect inadequate dispersion within the composite structure, potentially arising from insufficient fiber–matrix adhesion. The presence of voids and gaps in the SEM images further confirms this weak interfacial interaction. Effective fiber–matrix adhesion is essential to ensure efficient load transfer from the matrix to the fibers, thereby enhancing the strength and stiffness of the composite. The treatments applied to SCB fiber in this work may not have produced a sufficiently large or suitable surface area to achieve strong matrix–fiber bonding. Many studies has shown that the stress-strain behavior of natural-fiber-reinforced PLA composites follows strain-softening or viscoplastic behavior [13, 50, 65]. Mazzanti et al reported that PLA and PLA/hemp fiber biocomposites at 3 wt% hemp, both treated and untreated, exhibited a clear yield point followed by a strain softening and a stress plateau, whereas the composite with 6 wt% treated fiber showed purely elastic behavior [50]. According to Table 2, the fabricated composites in this study exhibit low tensile strength and medium flexible characteristic. Several studies have successfully fabricated reinforced PLA composites with a combination of high strength and flexibility. Previous work on PLA–MCC composites reported tensile strengths of 64–73 MPa and tensile moduli of 219–262 MPa, whereas neat PLA exhibited values of 67.35 MPa and 206 MPa, respectively [15]. Another PLA–based composite reinforced with pineapple leaf fibers achieved higher tensile strengths in the range of 85–101 MPa [21]. Bartos et al. prepared PLA/bagasse fiber composites, with and without a coupling agent, using a twin–screw compounding followed by injection molding; the resulting materials exhibited tensile strengths of 55–60 MPa and tensile moduli of 5.5–6.0 GPa [65]. However, a study on wood-sawdust-reinforced-PLA composite also exhibited low tensile strengths (7–8 MPa) and tensile moduli (350–450 MPa) [64].

3.7 | Antimicrobial Activity

Chitosan has been reported for having antimicrobial activity because it carries a positive charge at the C-2 position [66]. This positive charge can interact with the negative charges on the bacterial cell wall, causing physical damage to the wall, which leads to leakage of intracellular components and ultimately cell death [27]. The antibacterial activity of the specimen is presented in Table 3 as growth reduction percentage (%). Table 3 shows the absence of antibacterial activity shown by neat PLA,

27024288, 2026, 4, Downloaded from https://onlinelibrary.wiley.com/doi/10.1002/appl.70161 by Akbarningrum Fatmawati - Nat Prov Indonesia , Wiley Online Library on [18/08/2026]. See the Terms and Conditions (https://onlinelibrary.wiley.com/terms-and-conditions) on Wiley Online Library for rules of use; OA articles are governed by the applicable Creative Commons License

TABLE 3 | Bacterial counts and growth reduction from the antimicrobial assay.

Composite	*S. aureus*			*E. coli*		
	N_0, CFU/mL	N, CFU/mL	% R	N_0, CFU/mL	N, CFU/mL	% R
PLA	1.41×10^3	1.45×10^4	0	8.35×10^3	8.55×10^3	0
PLA–CS	1.41×10^3	1.36×10^4	3.55	8.35×10^3	9.75×10^3	0
PLA–CS–SCB	1.41×10^3	1.38×10^4	2.13	8.35×10^3	9.40×10^3	0
PLA–CS–UASCB	3×10^4	2.15×10^4	28.33	3×10^4	2.39×10^4	20.33
PLA–CS–UAASCB	3×10^4	2.18×10^4	27.33	3×10^4	2.68×10^4	10.67

PLA–CS, and PLA–CS–SCB specimens against Gram-negative *E. coli*. However, PLA–CS and PLA–CS–SCB specimens show very slight activity against Gram-positive *S. aureus*, whereas PLA still exhibits no activity against this strain, implying the contribution of CS to the antibacterial activity of the specimen. PLA–CS–UASCB shows nearly equal antibacterial effectiveness against both *S. aureus* and *E. coli*, suggesting a more balanced antibacterial action. PLA–CS–UAASCB also inhibits both bacteria, but its activity against *E. coli* is just under half of that observed against *S. aureus*, indicating reduced effectiveness against *E. coli*. These results suggest that adding treated fibers has a synergetic effect to chitosan, thereby improving the antibacterial activity of PLA–CS. The synergetic chitosan–cellulose interaction on antibacterial activity has been reported, attributing to the high surface area of cellulose that can adsorb antimicrobial compounds released from chitosan [67]. Bacterial cell adhesion to cellulose, facilitated by van der Waals and electrostatic interaction, has also been reported as attribution of antibacterial activity of cellulose [68]. Overall, the incorporation of chitosan into PLA still cannot provide the expected antibacterial activity. This phenomenon may be attributed to the depletion of $-NH_3^+$ within the matrix, which decreases the positive charge density and hinder its antibacterial activity [69, 70]. The water solubility and the pH used during the antibacterial assay may not support the antibacterial activity of the composite. To achieve the proper positive charge density for bactericidal activity the chitosan-based system should have a pH < 6.5, as described by Atay et al. [69] Furthermore, the active antimicrobial sites may be buried within the polymer bulk, preventing contact with the bacteria [71]. Thermal degradation of chitosan, which is highly susceptible to thermal decomposition and chain scission, during the composite fabrication may also result in reduced antibacterial activities, as described by Flores-León et al. [72].

4 | Conclusion

The reinforcement of PLA involving chitosan (CS), and either sugarcane bagasse (SCB), ultrasound-assisted-alkaline treated sugarcane bagasse (UASCB) or subsequent ultrasound-assisted-alkaline-acid treated sugarcane bagasse (UAASCB) was investigated in this study. The treatment successfully increased the cellulose content and the crystallinity of SCB. The Ultrasound-assisted-alkaline treatment using 4 wt% NaOH for 30 min increased the cellulose content from 43.2% to 58.2%, with crystallinity increasing from 64.7% to 88.95%, while the subsequent acid treatment using 2 N sulfuric acid further increased the cellulose to 71.7%. Despite these improvements in filler characteristics, the fabrication method still produced composites with large variation, low tensile strength, and moderate flexibility. The fabricated composites also showed low antibacterial activity under assay method used. Further optimization of the filler filament, composite processing, and antibacterial testing conditions is required to improve the mechanical performance and functional properties of these PLA-based composites.

Acknowledgments

The author sincerely acknowledges Chemical Engineering Department at Universitas Surabaya (UBAYA) for providing the academic environment, research facilities, and continuous support that enabled the completion of this work. This research activity was supported through RIIM kompetisi funding from the Indonesia Endowment Fund for Education Agency (LPDP), Ministry of Finance of the Republic of Indonesia and National Research and Innovation Agency of Indonesia (BRIN) according to the contract number 46/IV/KS/02/2025.

Conflicts of Interest

The authors declare no conflicts of interest.

Data Availability Statement

Data will be made on request.

References

1. R. A. Ilyas, S. M. Sapuan, M. M. Harussani, et al., "Polylactic Acid (PLA) Biocomposite: Processing, Additive Manufacturing and Advanced Applications," *Polymers* 13, no. 8 (2021): 1326, https://doi.org/10.3390/POLYM13081326.

2. F. D. Al-Shalawi, M. A. Azmah Hanim, M. K. A. Ariffin, et al., "Biodegradable Synthetic Polymer in Orthopaedic Application: A Review," *Materials Today: Proceedings* 74 (2023): 540–546, https://doi.org/10.1016/J.MATPR.2022.12.254.

3. Y. Matsuda, M. Karino, T. Okui, and T. Kanno, "Complications of Poly-L-Lactic Acid and Polyglycolic Acid (PLLA/PGA) Osteosynthesis Systems for Maxillofacial Surgery: A Retrospective Clinical Investigation," *Polymers* 13, no. 6 (2021): 889, https://doi.org/10.3390/POLYM13060889.

4. B. Parveez, M. S. Abu Bakar, A. Aabid, and M. Baig, "A Comprehensive Review of PLA-Blended Biocomposites and Their Application in Biomedical and Food Packagings," *Polymer-Plastics Technology and Materials* 63, no. 18 (2024): 2453–2483, https://doi.org/10.1080/25740881.2024.2375366.

5. V. DeStefano, S. Khan, and A. Tabada, "Applications of PLA in Modern Medicine," *Engineered Regeneration* 1 (2020): 76–87, https://doi.org/10.1016/J.ENGREG.2020.08.002.

27024288, 2026, 4, Downloaded from https://onlinelibrary.wiley.com/doi/10.1002/appl.70161 by Akbarningrum Fatmawati - Nat Prov Indonesia , Wiley Online Library on [18/08/2026]. See the Terms and Conditions (https://onlinelibrary.wiley.com/terms-and-conditions) on Wiley Online Library for rules of use; OA articles are governed by the applicable Creative Commons License

6. G. Narayanan, V. N. Vernekar, E. L. Kuyinu, and C. T. Laurencin, "Poly (Lactic Acid)-Based Biomaterials for Orthopaedic Regenerative Engineering," *Advanced Drug Delivery Reviews* 107 (2016): 247–276, https://doi.org/10.1016/J.ADDR.2016.04.015.

7. C. Gauss, K. L. Pickering, and L. P. Muthe, "The Use of Cellulose in Bio-Derived Formulations for 3D/4D Printing: A Review," *Composites Part C: Open Access* 4 (2021): 100113, https://doi.org/10.1016/J.JCOMC.2021.100113.

8. M. Elmeniawy, A. Mansour, A. Hamdy, and D. Saber, "Mechanical Properties and Corrosion Behavior of Sugarcane Bagasse Fiber Reinforced Low Density Polyethylene Composites," *The Egyptian International Journal of Engineering Sciences and Technology* 36, no. 2 (2021): 63–71, https://doi.org/10.21608/EIJEST.2021.80884.1072.

9. J. X. Sun, X. F. Sun, H. Zhao, and R. C. Sun, "Isolation and Characterization of Cellulose From Sugarcane Bagasse," *Polymer Degradation and Stability* 84, no. 2 (2004): 331–339, https://doi.org/10.1016/J.POLYMDEGRADSTAB.2004.02.008.

10. H. S. Kusuma, D. Permatasari, W. K. Umar, and S. K. Sharma, "Sugarcane Bagasse as an Environmentally Friendly Composite Material to Face the Sustainable Development Era," *Biomass Conversion and Biorefinery* 14, no. 21 (2024): 26693–26706, https://doi.org/10.1007/S13399-023-03764-2/METRICS.

11. M. Asrofi, R. R. Pradiza, M. Yusuf, M. Dominic C. D., and R. A. Ilyas, "Mechanical Properties of Biocomposite From Polylactic Acid and Natural Fiber and its Application: A Review Study," *Mechanical Engineering for Society and Industry* 5, no. 1 (2025): 52–61, https://doi.org/10.31603/MESI.12721.

12. D. Saber, M. A. El-meniawy, A. H. Abdelnaby, and A. M. Abdelhaleim, "Characterization of Reinforcing Polymeric Material With Recycled Sugarcane Bagasse Wastes as Fiber Natural Reinforcement," *Polymer Bulletin* 81, no. 16 (2024): 14767–14786, https://doi.org/10.1007/S00289-024-05409-4/METRICS.

13. M. Lubwama, O. Kirabo, M. Massooto, and V. A. Yiga, "Mechanical, Chemical, Biodegradability and Rheological Characteristics of Rice Husk Fibre-Reinforced PLA Bio-Composites," *Journal of Materials Science: Composites* 6, no. 1 (2025): 19, https://doi.org/10.1186/S42252-025-00084-8.

14. N. D. Ahmad, Kusmono, M. W. Wildan, and Herianto, "Preparation and Properties of Cellulose Nanocrystals-Reinforced Poly (Lactic Acid) Composite Filaments for 3D Printing Applications," *Results in Engineering* 17 (2023): 100842, https://doi.org/10.1016/J.RINENG.2022.100842.

15. X. Xian, X. Wang, Y. Zhu, Y. Guo, and Y. Tian, "Effects of MCC Content on the Structure and Performance of PLA/MCC Biocomposites," *Journal of Polymers and the Environment* 26, no. 8 (2018): 3484–3492, https://doi.org/10.1007/S10924-018-1226-3/METRICS.

16. M. H. Sarfraz, S. Hayat, M. H. Siddique, et al., "Chitosan Based Coatings and Films: A Perspective on Antimicrobial, Antioxidant, and Intelligent Food Packaging," *Progress in Organic Coatings* 188 (2024): 108235, https://doi.org/10.1016/J.PORGCOAT.2024.108235.

17. S. Ahmed, Annu, A. Ali, and J. Sheikh, "A Review on Chitosan Centred Scaffolds and Their Applications in Tissue Engineering," *International Journal of Biological Macromolecules* 116 (2018): 849–862, https://doi.org/10.1016/J.IJBIOMAC.2018.04.176.

18. F. Hong, P. Qiu, Y. Wang, et al., "Chitosan-Based Hydrogels: From Preparation to Applications, a Review," *Food Chemistry: X* 21 (2024): 101095, https://doi.org/10.1016/J.FOCHX.2023.101095.

19. I. Hui, E. Pasquier, A. Solberg, K. Agrenius, J. Håkansson, and G. Chinga-Carrasco, "Biocomposites Containing Poly(Lactic Acid) and Chitosan for 3D Printing - Assessment of Mechanical, Antibacterial and in Vitro Biodegradability Properties," *Journal of the Mechanical Behavior of Biomedical Materials* 147 (2023): 106136, https://doi.org/10.1016/J.JMBBM.2023.106136.

20. A. Fatmawati, R. Agustriyanto, and Y. Liasari, "Enzymatic Hydrolysis of Alkaline Pretreated Coconut Coir," *Bulletin of Chemical Reaction Engineering and Catalysis* 8, no. 1 (2013): 34–39, https://doi.org/10.9767/BCREC.8.1.4048.34-39.

21. J. Suteja, H. Firmanto, A. Soesanti, and C. Christian, "Properties Investigation of 3D Printed Continuous Pineapple Leaf Fiber-Reinforced PLA Composite," *Journal of Thermoplastic Composite Materials* 35, no. 11 (2022): 2052–2061, https://doi.org/10.1177/0892705720945371.

22. F. H. Ibrahim, R. A. Setiawan, S. Steven, and Y. Mardiyati, "Towards Sustainable Composites: Fabrication, Characterization, and Biodegradation of All-Cellulose Composites (ACC) From Ramie (Boehmeria Nivea) and Luffa (Luffa Cylindrica)," *Results in Engineering* 26 (2025): 104695, https://doi.org/10.1016/J.RINENG.2025.104695.

23. R. Datta, "Acidogenic Fermentation of Lignocellulose–Acid Yield and Conversion of Components," *Biotechnology and Bioengineering* 23, no. 9 (1981): 2167–2170, https://doi.org/10.1002/BIT.260230921.

24. A. Fatmawati, T. Nurtono, and A. Widjaja, "Thermogravimetric Kinetic-Based Computation of Raw and Pretreated Coconut Husk Powder Lignocellulosic Composition," *Bioresource Technology Reports* 22 (2023): 101500, https://doi.org/10.1016/J.BITEB.2023.101500.

25. X. Ju, M. Bowden, E. E. Brown, and X. Zhang, "An Improved X-Ray Diffraction Method for Cellulose Crystallinity Measurement," *Carbohydrate Polymers* 123 (2015): 476–481, https://doi.org/10.1016/J.CARBPOL.2014.12.071.

26. M. Mattonai, D. Pawcenis, S. del Seppia, J. Łojewska, and E. Ribechini, "Effect of Ball-Milling on Crystallinity Index, Degree of Polymerization and Thermal Stability of Cellulose," *Bioresource Technology* 270 (2018): 270–277, https://doi.org/10.1016/J.BIORTECH.2018.09.029.

27. P. Tyagi, R. Mathew, C. Opperman, et al., "High-Strength Antibacterial Chitosan-Cellulose Nanocrystal Composite Tissue Paper," *Langmuir* 35, no. 1 (2019): 104–112, https://doi.org/10.1021/acs.langmuir.8b02655.

28. L. V. Cabañas-Romero, C. Valls, S. V. Valenzuela, et al., "Bacterial Cellulose–Chitosan Paper With Antimicrobial and Antioxidant Activities," *Biomacromolecules* 21, no. 4 (2020): 1568–1577, https://doi.org/10.1021/ACS.BIOMAC.0C00127.

29. A. Fatmawati, N. Suseno, E. Savitri, G. T. Masui, and F. A. Ivony, "Chitosan-Based Coating Application to Enhance Antimicrobial and Water Vapor Barrier Properties of Industry-Manufactured Paper," *Journal Kimia Sains dan Aplikasi* 27, no. 11 (2024): 515–522, https://doi.org/10.14710/JKSA.27.11.515-522.

30. A. I. Gavrila, A. Vartolomei, I. Calinescu, et al., "Ultrasound-Assisted Alkaline Pretreatment of Biomass to Enhance the Extraction Yield of Valuable Chemicals," *Agronomy* 14, no. 5 (2024): 903, https://doi.org/10.3390/AGRONOMY14050903.

31. M. Vinatoru, T. J. Mason, and I. Calinescu, "Ultrasonically Assisted Extraction (UAE) and Microwave Assisted Extraction (MAE) of Functional Compounds From Plant Materials," *TrAC Trends in Analytical Chemistry* 97 (2017): 159–178, https://doi.org/10.1016/J.TRAC.2017.09.002.

32. I. Bagus, W. Gunam, N. M. Wartini, A. A. Made, D. Anggreni, and P. Komang Suparyana, "Delignifikasi Ampas Tebu Dengan Larutan Natrium Hidroksida Sebelum Proses Sakarifikasi Secara Enzimatis Menggunakan Enzim Selulase Kasar Dari Aspergillus Niger FNU 6018," *Jurnal Teknologi Indonesia* 34 (2011): 24–32.

33. J. Peng, R. Fu, Y. Huang, et al., "Influence and Mechanism of NaOH Concentration on the Dissolution of Cellulose and Extraction of CNF in Alkaline Solvents at 15°C," *Carbohydrate Polymers* 353 (2025): 123265, https://doi.org/10.1016/J.CARBPOL.2025.123265.

34. D. Tristantini and C. Sandra, "Synthesis of Cellulose Acetate from Palm Oil Bunches and Dried Jackfruit Leaves." *E3S Web Conf. Volume 67, The 3rd International Tropical Renewable Energy Conference "Sustainable Development of Tropical Renewable Energy" (i-TREC 2018)* (EDP Sciences, 2018). 67, 04035, https://doi.org/10.1051/e3sconf/20186704035.

27024288, 2026, 4, Downloaded from https://onlinelibrary.wiley.com/doi/10.1002/appl.70161 by Akbarningrum Fatmawati - Nat Prov Indonesia , Wiley Online Library on [18/08/2026]. See the Terms and Conditions (https://onlinelibrary.wiley.com/terms-and-conditions) on Wiley Online Library for rules of use; OA articles are governed by the applicable Creative Commons License

35. M. H. Mulla, M. N. Norizan, N. F. M. Rawi, M. H. M. Kassim, N. Abdullah, and M. N. F. Norrrahim, "Surface and Interfaces Effects of Concentrations and Alkaline Treatment Durations on Sugar Palm Fiber as Structural Reinforcement in Polymer Composites," *Journal of Natural Fibers* 22, no. 1 (2025): 2527277, https://doi.org/10.1080/15440478.2025.2527277.

36. S. P. Bangar, O. J. Esua, C. Nickhil, and W. S. Whiteside, "Microcrystalline Cellulose for Active Food Packaging Applications: A Review," *Food Package Shelf Life* 36 (2023): 101048, https://doi.org/10.1016/J.FPSL.2023.101048.

37. A. M. Adel, Z. H. Abd El-Wahab, A. A. Ibrahim, and M. T. Al-Shemy, "Characterization of Microcrystalline Cellulose Prepared From Lignocellulosic Materials. Part II: Physicochemical Properties," *Carbohydrate Polymers* 83, no. 2 (2011): 676–687, https://doi.org/10.1016/J.CARBPOL.2010.08.039.

38. M. S. Hasanin, N. Kassem, and M. L. Hassan, "Preparation and Characterization of Microcrystalline Cellulose From Olive Stones," *Biomass Conversion and Biorefinery* 13, no. 6 (2023): 5015–5022, https://doi.org/10.1007/S13399-021-01423-Y/METRICS.

39. M. P. Gundupalli, H. Kajiura, T. Ishimizu, and D. Bhattacharyya, "Alkaline Hydrolysis of Coconut Pith: Process Optimization, Enzymatic Saccharification, and Nitrobenzene Oxidation of Kraft Lignin," *Biomass Conversion and Biorefinery* 12, no. 7 (2022): 2349–2367, https://doi.org/10.1007/S13399-020-00890-Z/METRICS.

40. A. Abdulkhani, E. Hojati Marvast, A. Ashori, Y. Hamzeh, and A. N. Karimi, "Preparation of Cellulose/Polyvinyl Alcohol Biocomposite Films Using 1-n-Butyl-3-Methylimidazolium Chloride," *International Journal of Biological Macromolecules* 62 (2013): 379–386, https://doi.org/10.1016/J.IJBIOMAC.2013.08.050.

41. A. Koistinen, T. Vuorinen, and T. Maloney, "The Effect of Alkaline Pre-Treatment on Cellulose Pulp Fiber Dissolution," *Carbohydrate Polymer Technologies and Applications* 11 (2025): 100978, https://doi.org/10.1016/J.CARPTA.2025.100978.

42. M. S. Thomas, P. K. S. Pillai, M. Faria, et al., "Electrospun Polylactic Acid-Chitosan Composite: A Bio-Based Alternative for Inorganic Composites for Advanced Application," *Journal of Materials Science: Materials in Medicine* 29, no. 9 (2018): 137, https://doi.org/10.1007/S10856-018-6146-1/METRICS.

43. R. Hasnida Raja Hashim, A. Anas Nagoor Gunny, S. Sung Ting, N. Helya Iman Kamaludim, and S. C. B Gopinath, "The Effect of Nanofillers on the Functional Properties of PLA and Chitosan Based Film (Kesan Pengisian Nano Kepada Sifat Filem Yang Berasaskan Asid Polilatik Dan Kitosan)," *Malaysian Journal of Analytical Sciences* 27 (2023): 63–73.

44. L. Techawinyutham, R. S. Sundaram, I. Suyambulingam, et al., "Rice Husk Biowaste Derived Microcrystalline Cellulose Reinforced Sustainable Green Composites: A Comprehensive Characterization for Lightweight Applications," *International Journal of Biological Macromolecules* 299 (2025): 140153, https://doi.org/10.1016/J.IJBIOMAC.2025.140153.

45. K. Charoensopa, K. Thangunpai, P. Kong, T. Enomae, and W. Ploysri, "Extraction of Nanocellulose From the Residue of Sugarcane Bagasse Fiber for Anti-Staphylococcus aureus (*S. aureus*) Application," *Polymers* 16, no. 11 (2024): 1612, https://doi.org/10.3390/POLYM16111612.

46. A. Maslennikov, R. Peretz, V. K. Vadivel, and H. Mamane, "Recycled Paper Sludge (RPS)-Derived Nanocellulose: Production, Detection and Water Treatment Application," *Applied Sciences* 12, no. 6 (2022): 3077, https://doi.org/10.3390/APP12063077.

47. Z. Yuan, and X. R. Xu, "Surface Characteristics and Biotoxicity of Airborne Microplastics," *Comprehensive Analytical Chemistry* 100 (2023): 117–164, https://doi.org/10.1016/BS.COAC.2022.07.006.

48. K. S. Salem, N. K. Kasera, M. A. Rahman, et al., "Comparison and Assessment of Methods for Cellulose Crystallinity Determination," *Chemical Society Reviews* 52, no. 18 (2023): 6417–6446, https://doi.org/10.1039/D2CS00569G.

49. Y. Kong and J. N. Hay, "The Measurement of the Crystallinity of Polymers by DSC," *Polymer* 43, no. 14 (2002): 3873–3878, https://doi.org/10.1016/S0032-3861(02)00235-5.

50. V. Mazzanti, R. Pariante, A. Bonanno, O. Ruiz de Ballesteros, F. Mollica, and G. Filippone, "Reinforcing Mechanisms of Natural Fibers in Green Composites: Role of Fibers Morphology in a PLA/Hemp Model System," *Composites Science and Technology* 180 (2019): 51–59, https://doi.org/10.1016/J.COMPSCITECH.2019.05.015.

51. H. Y. Yu, H. Zhang, M. L. Song, Y. Zhou, J. Yao, and Q. Q. Ni, "From Cellulose Nanospheres, Nanorods to Nanofibers: Various Aspect Ratio Induced Nucleation/Reinforcing Effects on Polylactic Acid for Robust-Barrier Food Packaging," *ACS Applied Materials and Interfaces* 9, no. 50 (2017): 43920–43938, https://doi.org/10.1021/ACSAMI.7B09102/SUPPL_FILE/AM7B09102_SI_001.PDF.

52. U. K. Komal, M. K. Lila, and I. Singh, "PLA/Banana Fiber Based Sustainable Biocomposites: A Manufacturing Perspective," *Composites Part B: Engineering* 180 (2020): 107535, https://doi.org/10.1016/J.COMPOSITESB.2019.107535.

53. S. Gazzotti, R. Rampazzo, M. Hakkarainen, et al., "Cellulose Nanofibrils as Reinforcing Agents for PLA-Based Nanocomposites: An In Situ Approach," *Composites Science and Technology* 171 (2019): 94–102, https://doi.org/10.1016/J.COMPSCITECH.2018.12.015.

54. H. U. Ko, L. Zhai, J. H. Park, J. Y. Lee, D. Kim, and J. Kim, "Poly (Vinyl Alcohol)–Lignin Blended Resin for Cellulose-Based Composites," *Journal of Applied Polymer Science* 135, no. 34 (2018): 46655, https://doi.org/10.1002/APP.46655.

55. H. Hong, R. Xiao, Q. Guo, H. Liu, and H. Zhang, "Quantitively Characterizing the Chemical Composition of Tailored Bagasse Fiber and Its Effect on the Thermal and Mechanical Properties of Polylactic Acid-Based Composites," *Polymers* 11, no. 10 (2019): 1567, https://doi.org/10.3390/POLYM11101567.

56. M. Kowalczyk, E. Piorkowska, P. Kulpinski, and M. Pracella, "Mechanical and Thermal Properties of PLA Composites With Cellulose Nanofibers and Standard Size Fibers," *Composites Part A: Applied Science and Manufacturing* 42, no. 10 (2011): 1509–1514, https://doi.org/10.1016/J.COMPOSITESA.2011.07.003.

57. C. Wang, R. Zou, M. Qian, et al., "Improvement of the Carbon Yield From Biomass Carbonization Through Sulfuric Acid Pre-Dehydration at Room Temperature," *Bioresource Technology* 355 (2022): 127251, https://doi.org/10.1016/J.BIORTECH.2022.127251.

58. A. Banerjee, K. Jha, R. Kumar, et al., "Unveiling of Mechanical, Morphological, and Thermal Characteristics of Alkali-Treated Flax and Pine Cone Fiber-Reinforced Polylactic Acid (PLA) Composites: Fabrication and Characterizations," *Biomass Conversion and Biorefinery* 15, no. 8 (2025): 12043–12070, https://doi.org/10.1007/S13399-025-06496-7/METRICS.

59. T. C. Mokhena, J. S. Sefadi, E. R. Sadiku, M. J. John, M. J. Mochane, and A. Mtibe, "Thermoplastic Processing of PLA/Cellulose Nanomaterials Composites," *Polymers* 10, no. 12 (2018): 1363, https://doi.org/10.3390/POLYM10121363.

60. V. Slavković, B. Hanželič, V. Plesec, S. Milenković, and G. Harih, "Thermo-Mechanical Behavior and Strain Rate Sensitivity of 3D-Printed Polylactic Acid (PLA) below Glass Transition Temperature (Tg)," *Polymers* 16, no. 11 (2024): 1526, https://doi.org/10.3390/POLYM16111526/S1.

61. S. M. Mirkhalaf and M. Fagerström, "The Mechanical Behavior of Polylactic Acid (PLA) Films: Fabrication, Experiments and Modelling," *Mechanics of Time-Dependent Materials* 25, no. 2 (2021): 119–131, https://doi.org/10.1007/S11043-019-09429-W/FIGURES/10.

62. T. Zaharescu, M. Bumbac, C. M. Nicolescu, A. Craciun, and R. Mirea, "Oxidation Strength of PLA Filled With Algal Biomass and Rosemary Extract Powders for Food-Safe Handling," *Polymers* 18, no. 4 (2026): 504, https://doi.org/10.3390/POLYM18040504/S1.

27024288, 2026, 4, Downloaded from https://onlinelibrary.wiley.com/doi/10.1002/appl.70161 by Akbarningsum Fatmawati - Nat Prov Indonesia , Wiley Online Library on [18/08/2026]. See the Terms and Conditions (https://onlinelibrary.wiley.com/terms-and-conditions) on Wiley Online Library for rules of use; OA articles are governed by the applicable Creative Commons License

63. I. Velghe, B. Buffel, V. Vandeginste, W. Thielemans, and F. Desplentere, "Review on the Degradation of Poly(Lactic Acid) During Melt Processing," *Polymers* 15, no. 9 (2023): 2047, https://doi.org/10.3390/POLYM15092047.

64. N. Narlıoğlu, T. Salan, and M. H. Alma, "Properties of 3D-Printed Wood Sawdust-Reinforced PLA Composites," *Bioresources* 16, no. 3 (2021): 5467–5480, https://doi.org/10.15376/biores.16.3.5467-5480.

65. A. Bartos, K. Nagy, J. Anggono, et al., "Biobased PLA/Sugarcane Bagasse Fiber Composites: Effect of Fiber Characteristics and Interfacial Adhesion on Properties," *Composites Part A: Applied Science and Manufacturing* 143 (2021): 106273, https://doi.org/10.1016/J.COMPOSITESA.2021.106273.

66. T. Arifin, "Chitosan and Its Derivatives: Overlook of Commercial Application in Diverse Field." in *Chitosan: Derivatives, Composites and Applications*, eds. Shakeel Ahmed and Saiqa Ikram. (Wiley, 2017), 115–146.

67. T. Qu, X. Wang, and F. Zhang, "Antibacterial Food Packaging With Chitosan and Cellulose Blends for Food Preservation," *Polymers* 17, no. 13 (2025): 1850, https://doi.org/10.3390/POLYM17131850.

68. M. D. Onofrei, A. M. Dobos, S. Dunca, E. G. Ioanid, and S. Ioan, "Biocidal Activity of Cellulose Materials for Medical Implants," *Journal of Applied Polymer Science* 132 (2015): 41932, https://doi.org/10.1002/APP.41932.

69. H. Yilmaz Atay, "Antibacterial Activity of Chitosan-Based Systems," in *Functional Chitosan*, ed. S. Jana and S. Jana, (Springer, 2019), https://doi.org/10.1007/978-981-15-0263-7_15.

70. A. R. Egorov, A. A. Kirichuk, V. V. Rubanik, Jr Rubanik, VV, A. G. Tskhovrebov, and A. S. Kritchenkov, "Chitosan and its Derivatives: Preparation and Antibacterial Properties," *Materials (Basel, Switzerland)* 16, no. 18 (2023): 6076, https://doi.org/10.3390/MA16186076.

71. L. Suryanegara, W. Fatriasari, D. Zulfiana, et al., "Novel Antimicrobial Bioplastic Based on PLA-Chitosan by Addition of TiO2 and ZnO," *Journal of Environmental Health Science and Engineering* 19, no. 1 (2021): 415–425, https://doi.org/10.1007/S40201-021-00614-Z/FIGURES/8.

72. J. R. Flores-León, D. E. Rodríguez-Félix, J. M. Quiroz-Castillo, et al., "Effect of Degradation on the Physicochemical and Mechanical Properties of Extruded Films of Poly(Lactic Acid) and Chitosan," *ACS Omega* 9, no. 8 (2024): 9526–9535, https://doi.org/10.1021/ACSOMEGA.3C09296/ASSET/IMAGES/LARGE/AO3C09296_0010.JPEG.

27024288, 2026, 4, Downloaded from https://onlinelibrary.wiley.com/doi/10.1002/appl.70161 by Akbarningrum Fatmawati - Nat Prov Indonesia , Wiley Online Library on [18/08/2026]. See the Terms and Conditions (https://onlinelibrary.wiley.com/terms-and-conditions) on Wiley Online Library for rules of use; OA articles are governed by the applicable Creative Commons License